

Photochemical and Thermal Reactions of Intermediates in the Phenylnitrene Rearrangement Inside a Hemicarcerand

Ralf Warmuth* and Slawomir Makowiec

Contribution from the Department of Chemistry and Chemical Biology, Rutgers,
The State University of New Jersey, Piscataway, New Jersey 08854

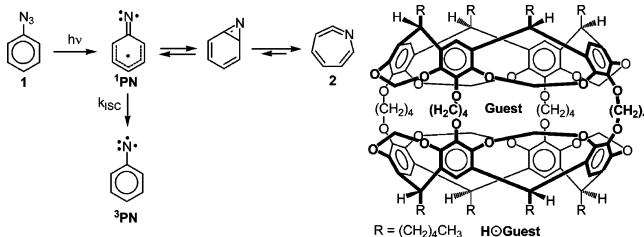
Received August 23, 2006; E-mail: warmuth@rutgers.edu

Abstract: Broadband irradiation ($\lambda > 320$ nm) of hemicarceplex **H**⊙**1** between -74 °C and -84 °C, produces encapsulated didehydroazepine (**2**), triplet phenylnitrene (^3PN), 2-azabicyclo[3.2.0]hepta-1,3,6-triene (**6**), and 4-azaspiro[2.4]hepta-1,4,6-triene (**7**). The highly strained anti-Bredt imine **6** is formed from **2** via a photochemical four-electron electrocyclization. Under the irradiation conditions, **6** rearranges further to azaspiroene **7**. In addition, **6** thermally rearranges to **7** via a 1,5-sigmatropic shift ($\Delta G^\ddagger_{267\text{K}} = 20.0 \pm 0.5$ kcal/mol), yielding a final equilibrium composed of $[\mathbf{7}]/[\mathbf{6}] = 5$ at room temperature. The observation of a photochemical rearrangement of **2** to **6** contrasts earlier results of narrow band irradiations ($\lambda = 334$ nm) of matrix-isolated **2**, which gave ^3PN (Hayes, J. C.; Sheridan, R. S. *J. Am. Chem. Soc.* **1990**, *112*, 5879–5881). Encapsulated ^3PN is remarkably stable due to the prevention of its dimerization by the surrounding hemicarcerand. Above 255 K, it slowly decays with a rate constant $k = 10^{7.7 \pm 0.4} \text{ s}^{-1} \times \exp \{ (13300 \pm 500 \text{ cal/mol})/RT \}$. The isolation of substantial amounts of a hemicarcerand lacking one acetal spanner suggests that ^3PN decays preferentially by inserting into an inward-pointing acetal C–H bond of **H**.

Introduction

Aryl azides have important applications in photolithography, polymer chemistry, and photoaffinity labeling of biomolecules.¹ Photolysis of the parent phenyl azide (**1**) produces singlet phenylnitrene (^1PN). Above 165 K, ^1PN ring-expands to didehydroazepine (**2**).² At lower temperature, ^1PN preferentially intersystem crosses to triplet phenylnitrene (^3PN) (Scheme 1). Much of our knowledge about the mechanistic details of the phenylnitrene rearrangement and about the properties and

Scheme 1. Photochemistry of Phenylazide



reactivities of participating intermediates has come from matrix isolation studies,^{3–8} time-resolved spectroscopy,^{9–14} and high level ab initio calculations.^{15,16}

Recently, synthetic host molecules have been applied to investigate arylnitrene rearrangements and their intermediates.^{17–19} Bucher et al. incorporated an aryl azide unit into the molecular

- (1) (a) Breslow, D. S. In *Azides and Nitrenes*; Scriven, E. F. U., Ed.; Academic Press: New York, 1984; Vol. 491. (b) Bayley, H. *Photogenerated Reagents in Biochemistry and Molecular Biology*; Elsevier: Amsterdam, 1983.
- (2) (a) Schuster, G. B.; Platz, M. S. *Adv. Photochem.* **1992**, *17*, 69–143. (b) Gritsan, N. P.; Pritchina, E. A. *Russ. Chem. Rev.* **1992**, *61*, 500–516. (c) Platz, M. S. *Acc. Chem. Res.* **1995**, *28*, 487–492. (d) Borden, W. T.; Gritsan, N. P.; Hadad, C. M.; Karney, W. L.; Kemnitz, C. R.; Platz, M. S. *Acc. Chem. Res.* **2000**, *33*, 765–771.
- (3) (a) Smolinsky, G.; Wasserman, E.; Yager, W. A. *J. Am. Chem. Soc.* **1962**, *84*, 3220–3221. (b) Reiser, A.; Frazer, V. *Nature (London)* **1965**, *208*, 682–683.
- (4) (a) Chapman, O. L.; Le Roux, J.-P. *J. Am. Chem. Soc.* **1978**, *100*, 282–285. (b) Chapman, O. L.; Sheridan, R. S.; Le Roux, J.-P. *J. Am. Chem. Soc.* **1978**, *100*, 6245–6247.
- (5) Hayes, J. C.; Sheridan, R. S. *J. Am. Chem. Soc.* **1990**, *112*, 5879–5881.
- (6) Dunkin, I. R.; Lynch, M. A.; McAlpine, F.; Sweeney, D. J. *Photochem. Photobiol., A* **1997**, *102*, 207–212.
- (7) (a) Waddell, W. H.; Feilchenfeld, N. B. *J. Am. Chem. Soc.* **1983**, *105*, 5499–5500. (b) Leyva, E.; Platz, M. S.; Persy, G.; Wirz, J. *J. Am. Chem. Soc.* **1986**, *108*, 3783–3790.
- (8) Morawietz, J.; Sander, W. *J. Org. Chem.* **1996**, *61*, 4351–4354.
- (9) Leyva, E.; Platz, M. S.; Persy, G.; Wirz, J. *J. Am. Chem. Soc.* **1986**, *108*, 3783–3790.
- (10) (a) Schrock, A. K.; Schuster, G. B. *J. Am. Chem. Soc.* **1984**, *106*, 5228–5234. (b) Shields, C. J.; Chrisope, D. R.; Schuster, G. B.; Dixon, A. J.; Poliakov, M.; Turner, J. J. *J. Am. Chem. Soc.* **1987**, *109*, 4723–4726. (c) Li, Y.-Z.; Kirby, J. P.; George, M. W.; Poliakov, M.; Schuster, G. B. *J. Am. Chem. Soc.* **1988**, *110*, 8092–8098.
- (11) (a) Gritsan, N. P.; Yuzawa, T.; Platz, M. S. *J. Am. Chem. Soc.* **1997**, *119*, 5059–5060. (b) Gritsan, N. P.; Zhu, Z.; Hadad, C. M.; Platz, M. S. *J. Am. Chem. Soc.* **1999**, *121*, 1202–1207.

- (12) Rizk, M. S.; Shi, X.; Platz, M. S. *Biochemistry* **2006**, *45*, 543–551.
- (13) (a) Gritsan, N. P.; Zhai, H. B.; Yuzawa, T.; Karweik, D.; Brooke, J.; Platz, M. S. *J. Phys. Chem. A* **1997**, *101*, 2833–2840. (b) Gritsan, N. P.; Tigelaar, D.; Platz, M. S. *J. Phys. Chem. B* **1999**, *103*, 4465–4469. (c) Gritsan, N. P.; Gudmundsdóttir, A. D.; Tigelaar, D.; Platz, M. S. *J. Phys. Chem. A* **1999**, *103*, 3458–3461.
- (14) (a) Gritsan, N. P.; Likhovotrik, I.; Tsao, M.-L.; Celebi, N.; Platz, M. S.; Karney, W. L.; Kemnitz, C. R.; Borden, W. T. *J. Am. Chem. Soc.* **2001**, *123*, 1425–1433. (b) Gritsan, N. P.; Gudmundsdóttir, A. D.; Tigelaar, D.; Zhu, Z.; Karney, W. L.; Hadad, C. M.; Platz, M. S. *J. Am. Chem. Soc.* **2001**, *123*, 1951–1962.
- (15) (a) Hrovat, D.; Waali, E. E.; Borden, W. T. *J. Am. Chem. Soc.* **1992**, *114*, 8698–8699. (b) Karney, W. L.; Borden, W. T. *J. Am. Chem. Soc.* **1997**, *119*, 1378–1387. (c) Kemnitz, C. R.; Karney, W. L.; Borden, W. T. *J. Am. Chem. Soc.* **1998**, *120*, 3499–3503. (d) Tsao, M.-L.; Platz, M. S. *J. Am. Chem. Soc.* **2003**, *125*, 12014–12025.
- (16) Karney, W. L.; Borden, W. T. *J. Am. Chem. Soc.* **1997**, *119*, 3347–3350.
- (17) Tokitoh, N.; Saiki, T.; Okazaki, R. *Chem. Commun.* **1995**, 1899–1900.
- (18) (a) Tönshoff, C.; Bucher, G. *Eur. J. Org. Chem.* **2004**, 269–271. (b) Bucher, G.; Tönshoff, C.; Nicolaides, A. *J. Am. Chem. Soc.* **2005**, *127*, 6883–6892.
- (19) Warmuth, R.; Makowiec, S. *J. Am. Chem. Soc.* **2005**, *127*, 1084–1085.

frame of a cryptand such that the azide functional group pointed into the protective cavity of the host. Photolysis produced a remarkably stable singlet arylnitrene.^{18b} In a previous communication, we reported the use of hemicarcerand **H** to investigate the phenylnitrene rearrangement.¹⁹ The inner phases of hemicarcerands are superb environments for the stabilization and spectroscopic characterization of reactive intermediates.^{20–22} If a reactive species is generated photochemically inside a hemicarcerand, it is protected from dimerization or the reaction with bulk-phase reactants by the surrounding host, allowing its observation under ordinary working conditions. Photolysis of the phenylazide hemicarceplex **H**⊙**1** produced the highly strained encapsulated didehydroazepine **2**, whose ¹³C NMR spectrum could be recorded (Scheme 1). We were also able to determine the barrier for the ring-contraction of **2** leading back to phenylnitrene. During our investigation we noticed that yields of encapsulated **2** strongly depended on the photolysis conditions and decreased upon prolonged irradiation with the simultaneous formation of new photoproducts. Good yields could only be obtained at low conversion. The work described here aims at elucidating the photochemical behavior of **2** in the inner phase of **H**. Even though the photoreactivity of **2** has been studied in inert gas matrices,^{4,5} the photoreactions reported here differ from those observed in earlier matrix studies and might be unique to inner phases. We also address the properties and reactivity of encapsulated triplet ³PN, which is generated together with **2** during the inner phase photolysis of **1**. In fact, encapsulation strongly increases the lifetime of the otherwise fleeting ³PN.²³

Experimental Section

General. ¹H NMR and ¹³C NMR spectra were recorded on 400 and 300 MHz Varian NMR spectrometer. ¹H (¹³C) NMR spectra taken in CDCl₃ or CD₂Cl₂ were referenced to residual CHCl₃ and CDHCl₂ at δ 7.26 (77.0) and 5.30 (54.0) respectively. The temperature of the NMR spectrometer was calibrated with a methanol standard using calibration curves implemented in the Varian NMR software. Mass spectra were recorded on an Applied Biosystems Voyager DE-Pro mass spectrometer in reflectron mode (MALDI-TOF). 2,4,6-Trihydroxylacetophenone (THAP) was used as matrix.

The synthesis of hemicarceplexes **H**⊙**1** and **H**⊙¹³C₆-**1** has been described earlier.¹⁹

NMR Experiments. In a typical experiment a solution of **H**⊙**1** (4–5 mg) or **H**⊙¹³C₆-**1** (15–17 mg) in the deuterated solvent (mixture), (450–500 μL) was placed in a pyrex NMR tube and degassed by four freeze–pump–thaw cycles under vacuum. The NMR tube was sealed under vacuum. The sample was irradiated for 7–15 min with the output

of an Oriel 200 W Hg Power-Max lamp. A 10 cm water filter and a 320 nm cutoff filter (WG320) was placed between the lamp and the sample. The sample tube was immersed in methanol, which was chilled with an immersion cooler in a partially silvered dewar flask. The temperature was measured with a thermocouple. After irradiation, the sample was cooled to –95 °C and subsequently inserted into the precooled probe of the NMR spectrometer.

UV/Vis Experiments. In a typical experiment a degassed solution of **H**⊙**1** (3 mg/mL) in CH₂Cl₂ was injected under Argon into a homemade low-temperature UV cell. This cell consists of a Viton O-ring (12.4 mm inner diameter; 2.6 mm thick) sandwiched between two 0.5 mm thick sapphire windows, which are mounted and pressed together in a commercial cryostat IR window holder. The cell was mounted on the top of the expander of a Cryogenics Closed Cycle Laboratory System Model CWS-202 (APD Cryogenics). After evacuation of the system, the cell was cooled to between 260 and 183 K. The temperature was measured with a thermocouple, which was fixed to one of the sapphire windows. UV spectra were recorded with a Shimadzu 2401 UV/vis spectrophotometer. The sample was irradiated through a Pyrex light guard and a WG320 cutoff filter with the output of an Oriel 200 W Hg Power-Max lamp (10–20 min). Rate constants *k*_{obs} for the decay of **H**⊙³PN were determined from the time-dependent change of the absorption at 388 and 412 nm. Every 4.5 s (above 260 K) or 9 s (at or below 260 K), a data point was collected.

Hemicarcerand 8. Isolated from the crude photolysis mixture by semipreparative HPLC (Phenomenex; SiO₂; 10 × 250 mm; CH₂Cl₂ containing 0.3 vol % THF; retention time = 24.3 min). ¹H NMR (300 MHz; CDCl₃; 23 °C): δ 7.57 (s, 2H, OH), 6.89 (s, 2H, aryl-H), 6.79 (s, 2H, aryl-H), 6.76 (s, 2H, aryl-H), 6.75 (s, 2H, aryl-H), 5.92 (d, 1H, ³J = 7.3 Hz, OCHH_{outer}O), 5.85 (d, 3H, ³J = 6.9 Hz, OCHH_{outer}O), 5.75 (d, 2H, ³J = 7.2 Hz, OCHH_{outer}O), 5.61 (d, 1H, ³J = 6.9 Hz, OCHH_{outer}O), 4.78–4.57 (m, 7H, CHCH₂(CH₂)₃CH₃), 4.57–4.44 (m, 3H, 1 CHCH₂(CH₂)₃CH₃, 2 OCH₂CH₂), 4.26 (d, 2H, ³J = 6.9 Hz, OCHH_{inner}O), 4.24–4.08 (m, 7H, 5OCHH_{inner}O, 2 OCH₂CH₂), 4.07–3.95 (m, 4H, OCH₂CH₂), 3.90–3.63 (m, 8H, OCH₂CH₂), 2.35–1.77 (m, 32H, 16OCH₂CH₂, 16CHCH₂(CH₂)₃CH₃), 1.54–1.10 (m, 48H, CHCH₂CH₂CH₂CH₂CH₃), 1.04–0.8 (m, 24H, CH₃); ¹³C NMR (75.4 MHz; CDCl₃; 23 °C): δ 148.31, 148.01, 147.99, 147.92, 147.88, 147.30, 147.00, 144.50, 143.96, 143.41, 143.32, 138.70, 138.51, 138.47, 138.19, 138.17, 138.01, 133.09, 127.87, 115.95, 114.08, 113.61, 112.97, 100.26, 100.04, 99.62, 99.33, 99.04, 74.39, 74.13, 73.88, 72.91, 36.70, 36.47, 36.30, 34.88, 33.06, 31.89, 31.87, 31.84, 31.76, 31.52, 30.39, 29.85, 29.71, 29.49, 27.85, 27.45, 27.43, 27.31, 27.20, 27.16, 27.04, 26.49, 22.55, 22.49, 22.47, 22.46, 22.41, 13.96, 13.95, 13.95, 13.92; MALDI-TOF: *m/z* 1967.19 ([M + H]⁺, 48%; calc 1967.08), 1989.30 ([M – Na]⁺, 100%; calc 1989.06).

Computational Methods. All calculation were carried out with the program *Gaussian 03*.²⁴ All geometries were optimized by the DFT approach²⁵ using the three-parameter hybrid functional B3LYP^{26–27} with a 6-31G(d) basis set.²⁸ The geometries of **2**, **6**, **7**, **17**, **18**, tetramethylsilane (TMS) and benzene and those of transition states **TS**_{2–6}, **TS**_{6–7}, **TS**_{6–17}, and **TS**_{17–18} were further optimized at the B3LYP level with the 6-311G(d) basis set.²⁹ Correlation between each transition state and the corresponding reactants and products was confirmed with IRC calculations at the B3LYP level of theory with the 6-311G(d) basis

- (20) (a) Warmuth, R. *J. Inclusion Phenom.* **2000**, *37*, 1–38. (b) Warmuth, R. *Eur. J. Org. Chem.* **2001**, 423–437. (c) Kirmse, W. *Angew. Chem., Int. Ed.* **2005**, *45*, 2476–2479.
- (21) (a) Cram, D. J.; Tanner, M. E.; Thomas, R. *Angew. Chem., Int. Ed.* **1991**, *30*, 1024–1027. (b) Warmuth, R. *Angew. Chem., Int. Ed.* **1997**, *36*, 1347–1350. (c) Warmuth, R. *Chem. Commun.* **1998**, 59–60. (d) Warmuth, R.; Marvel, M. A. *Angew. Chem., Int. Ed.* **2000**, *39*, 1117–1119. (e) Warmuth, R.; Marvel, M. A. *Chem. Eur. J.* **2001**, *7*, 1209–1220. (f) Warmuth, R. *J. Am. Chem. Soc.* **2001**, *123*, 6955–6956. (g) Kerdelhué, J.-L.; Langenwalter, K. J.; Warmuth, R. *J. Am. Chem. Soc.* **2003**, *125*, 973–986. (h) Makeiff, D. A.; Vishnumurthy, K.; Sherman, J. C. *J. Am. Chem. Soc.* **2003**, *125*, 9558–9559. (i) Roach, P.; Warmuth, R. *Angew. Chem., Int. Ed.* **2003**, *42*, 3039–3042. (j) Li, X.; Chu, G.; Moss, R. A.; Sauer, R. R.; Warmuth, R. *Angew. Chem., Int. Ed.* **2005**, *44*, 1994–1997.
- (22) For stabilization of reactive species in other molecular capsules see: (a) Ziegler, M.; Brumaghim, J. L.; Raymond, K. N. *Angew. Chem., Int. Ed.* **2000**, *39*, 4119–4121. (b) Körner, S. K.; Tucci, F. C.; Rudkevich, D. M.; Heinz, T.; Rebek, J., Jr. *Chem. Eur. J.* **2000**, *6*, 187–195. (c) Yoshizawa, M.; Kusukawa, T.; Fujita, M.; Sakamoto, S.; Yamaguchi, K. *J. Am. Chem. Soc.* **2001**, *123*, 10454–10459. (d) Kawano, M.; Kobayashi, Y.; Ozeki, T.; Fujita, M. *J. Am. Chem. Soc.* **2006**, *128*, 6558–6559.
- (23) For highly stabilized triplet nitrenes encapsulated in polymeric matrices see: Reiser, A.; Leyshon, L. *J. Am. Chem. Soc.* **1970**, *92*, 7487.

- (24) Frisch, M. J.; et al. *Gaussian 03*, Revision B.02; Gaussian, Inc.: Pittsburgh PA, 2003.
- (25) Hehre, W. J.; Radom, L.; Schleyer, P. v. R.; Pople, J. A. *Ab Initio Molecular Orbital Theory*; Wiley: New York, 1986.
- (26) (a) Becke, A. D. *Phys. Rev. A* **1988**, *38*, 3098–3100. (b) Becke, A. D. *J. Chem. Phys.* **1993**, *98*, 5648–52.
- (27) Lee, C.; Yang, W.; Parr, R. G. *Phys. Rev. B* **1988**, *37*, 785–789.
- (28) Hariharan, P. C.; Pople, J. A. *Theor. Chim. Acta* **1973**, *28*, 213–222.
- (29) (a) McLean, A. D.; Chandler, G. S. *J. Chem. Phys.* **1980**, *72*, 5639–5648. (b) Krishnan, R.; Binkley, J. S.; Seeger, R.; Pople, J. A. *J. Chem. Phys.* **1980**, *72*, 650–654. (c) Clark, T.; Chandrasekhar, J.; Spitznagel, G. W.; Schleyer, P. v. R. *J. Comput. Chem.* **1983**, *4*, 294–301. (d) Frisch, M. J.; Pople, J. A.; Binkley, J. S. *J. Chem. Phys.* **1984**, *80*, 3265–3269.

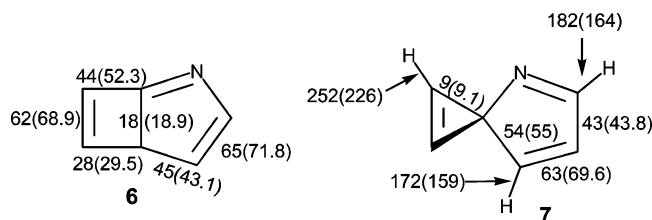


Figure 2. Experimental and computed (in parenthesis, PBE1PBE/6-311G++(2d, p)) homo- and heteronuclear coupling constants $^1J_{CC}$ and $^1J_{CH}$ (in Hz) of **6** and **7**.

Table 2. Selected Observed and Calculated (B3LYP/6-311G(d)) IR Frequencies (in cm^{-1}) of Encapsulated **1**, **2**, **6**, and **7**

stretch	ν (calc)	ν (scaled) ^a	ν (exptl)	ref
$\nu_{N=N}(\mathbf{1})$	2249.1	2136.6	2121.7	19
$\nu_{C=C=N}(\mathbf{2})$	1960.4	1862.4	1886	19
$\nu_{C=N}(\mathbf{6})$	1598.4	1518.5	n.d. ^b	
$\nu_{C=N}(\mathbf{7})$	1577.8	1499	n.d. ^b	
$\nu_{C=C}(\text{cyclopropene})(\mathbf{7})$	1757.8	1669.9	1665	

^a Scaled by 0.95 ^b Not detected. Our IR cell is only suitable for the observation of IR absorptions above 1600 cm^{-1} .

sev et al. recently postulated the corresponding benzannulated derivatives of **3–5** as possible photoproducts of a matrix-isolated benzannulated didehydroazepine.³⁴ However, GIAO ^{13}C chemical shifts calculations (PBE1PBE/6-311G++(2d, p)) using the B3LYP/6-311G(d) optimized structures of **3–5** did not match the measured ^{13}C chemical shifts of **A** and **B**, which exclude a photochemical ring-opening reaction of **2**. On the other hand, very good agreement between calculated and measured chemical shifts were observed for 2-azabicyclo[3.2.0]hepta-1,3,6-triene (**6**) and 4-azaspiro[2.4]hepta-1,4,6-triene (**7**), which we assign to guests **A** and **B**, respectively (Table 1). The bridgehead imine **6** is the expected product of the photochemically allowed four-electron electrocyclization of **2** and rearranges thermally to azaspiro **7** via a 1,5-sigmatropic shift (Scheme 2).

Also consistent with the assigned structures of **6** and **7** are the measured direct $^{13}\text{C}–^{13}\text{C}$ and $^{13}\text{C}–^1\text{H}$ coupling constants, which are in the range of those observed for compounds with similar C–C and C–H bonds,^{35–36} and which compare excellently with those computed using DFT methods (PBE1PBE/6-311G++(2d, p)) (see Figure 2 and Table S2). Especially characteristic for **7** are the direct coupling between the spiro carbon and the two equivalent cyclopropene carbons $^1J_{CC} = 9\text{ Hz}$ and the cyclopropene C–H coupling $^1J_{CH} = 252\text{ Hz}$. Further evidence for **7** as the final product of the rearrangement **2** \rightarrow **6** \rightarrow **7** comes from FT–IR spectroscopy. The cyclopropene C=C stretch of **7** was observed at $\nu(\text{C}=\text{C}) = 1665.2\text{ cm}^{-1}$, which is in good agreement with the scaled calculated frequency of 1669.9 cm^{-1} (Table 2).

The thermal interconversion of **H@6** and **H@7** could also be observed by ^1H NMR spectroscopy. Partial ^1H NMR spectra of **H@1** in CD_2Cl_2 after irradiation at $-83\text{ }^\circ\text{C}$ and warm-up to $-5\text{ }^\circ\text{C}$ are shown in Figure 3. The two multiplets at δ 3.24, 3.30, and 3.42 slowly decreased in intensity with a rate ($k =$

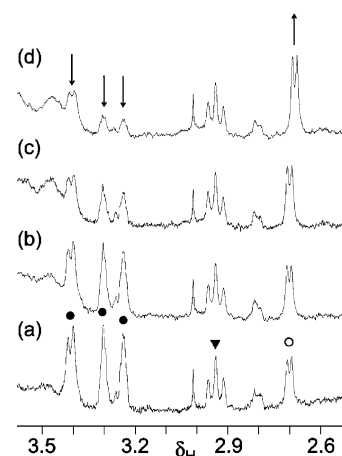


Figure 3. Partial ^1H NMR spectra (300 MHz; CD_2Cl_2 , $-5\text{ }^\circ\text{C}$) of an irradiated solution of **H@1** immediately (a), 9 min (b), 41 min (c) and 2 h (d) after warming the solution from the photolysis temperature ($-84\text{ }^\circ\text{C}$) to $-5\text{ }^\circ\text{C}$. Signals assigned to protons of **1** (▼), **6** (○), and **7** (●) are marked.

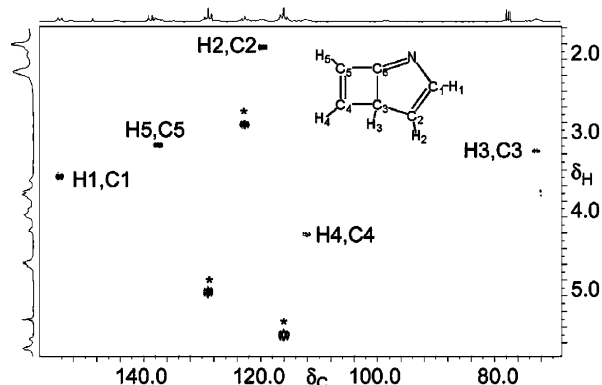


Figure 4. HETCOR (100 MHz; $\text{CD}_2\text{Cl}_2/\text{CDCl}_3$, 4:1; 243 K) of an irradiated solution of **H@ $^{13}\text{C}_6$ -1**. ^1H , ^{13}C cross correlations of encapsulated $^{13}\text{C}_6$ -**6** are labeled. Cross correlations of unphotolyzed, encapsulated $^{13}\text{C}_6$ -**1** are marked with asterisks.

$3.3 \times 10^{-4}\text{ s}^{-1}$), which is comparable to the rate observed by ^{13}C NMR for the rearrangement **H@ $^{13}\text{C}_6$ -6** to **H@ $^{13}\text{C}_6$ -7**. The multiplets are assigned to three protons of guest **6**. At the same time, the intensity of the doublet at δ 2.70 increased by the same amount and is assigned to one proton of guest **7**.

A complete assignment of all ^1H signals of **6** and **7**, which are partially covered by host signals, was possible via HETCOR experiments (Figures 4 and 5; see also Table 1). In the low-temperature HETCOR of a solution containing primarily **H@ $^{13}\text{C}_6$ -6**, five cross correlations between the carbon multiplets of **6** at δ 154.4, 137.5, 119.6, 112.2, and 73.0 and ^1H multiplets at δ 3.50 (d), 3.09 (bs), 1.85, 4.22, and 3.16 (bs) were observed (Figure 4). On this basis, we assign the latter to H1, H5, H2, H4, and H3 of **6**, respectively. The HETCOR of the same solution after the **6** to **7** rearrangement allowed us to assign the four chemically different protons H1, H2, H3, and H4/H5 of **7** to multiplets at δ 4.74, 2.79 (d), 5.2s (d), and 5.54 (s), respectively (Figure 5). These assignments were further supported by low ($-79.5\text{ }^\circ\text{C}$)- and room-temperature $^1\text{H}–^1\text{H}$ TOCSY and $^1\text{H}–^1\text{H}$ DQCOSY experiments, which showed the expected cross-correlations between the protons of encapsulated **6** and **7** (Figures S1–S3 in SI). Table 1 summarizes experimental ^1H chemical shifts δ_{exp} of encapsulated **6** and **7**,

(34) Maltsev, A.; Bally, T.; Tsao, M.-L.; Platz, M. S.; Kuhn, A.; Vosswinkel, M.; Wentrup, C. *J. Am. Chem. Soc.* **2004**, *126*, 237–249.

(35) Guenther, H. *NMR Spectroscopy*, 3rd ed.; George Thieme Verlag: New York, 1992.

(36) The $^{13}\text{C}–^1\text{H}$ coupling constants of $^{13}\text{C}_6$ -**7** were determined from a proton-coupled ^{13}C NMR spectrum (100 MHz; $\text{CD}_2\text{Cl}_2/\text{CDCl}_3$ (6:1); 298 K) of a solution containing **H@ $^{13}\text{C}_6$ -7**.

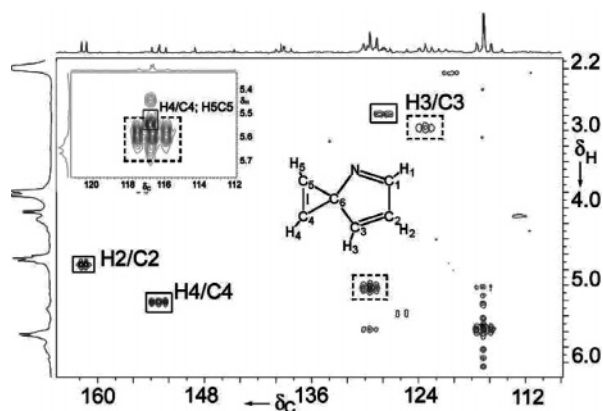


Figure 5. HETCOR (100 MHz; $\text{CD}_2\text{Cl}_2/\text{CDCl}_3$, 6:1; 298 K) of an irradiated solution of $\text{H}\odot^{13}\text{C}_6\text{-1}$. ^1H , ^{13}C cross correlations of encapsulated $^{13}\text{C}_6\text{-7}$ and $^{13}\text{C}_6\text{-1}$ are marked with unbroken and dashed lines, respectively.

calculated chemical shifts δ_{calc} and predicted hemicarcerand-induced upfield shifts $\Delta\delta = \delta_{\text{calc}} - \delta_{\text{exp}}$.

Attempts to isolate and purify hemicarceplex $\text{H}\odot\text{7}$ by silica gel column chromatography failed due to the acid sensitivity of the guest.³⁷ Instead, an equivalent amount of empty hemicarcerand **H** was eluted from the column (typically 30–40% yield based on consumed $\text{H}\odot\text{1}$ at >50% conversion). The decomposition of **7** presumably proceeds via initial acid-catalyzed hydrolysis of the imine. Subsequent protonation of the amino group of the hydrolysis product will facilitate its escape from the inner cavity of **H**.³⁸ Diol host **8**, which lacks one acetal spanner, was the second major isolated product (20–30%, Chart 1). The identity of **8** is supported by comparing its spectroscopic properties with those of an authentic sample, which was prepared as described earlier.^{38b} We reckon that diol host **8** is formed via hydrolysis of *N*-anilino-orthoformamide **9**. The latter is the expected product of the innermolecular insertion of **PN** into an inward-pointing acetal C–H bond of **H**. Since we were unable to identify signals of **8** in the ^1H NMR spectrum of the crude photolysis mixture, we believe that **9** hydrolyzed during the silica gel column chromatography.

Potential Energy Surface of the $2 \rightarrow 6 \rightarrow 7$ Rearrangement. Optimized structures and relative energies (B3LYP/6-311G(d)) of **2**, **6**, and **7** as well as of the transition states $\text{TS}_{2 \rightarrow 6}$ and $\text{TS}_{6 \rightarrow 7}$ that connect the three local minima are shown in Figure 6. On the basis of these calculations, it is not expected that **6**, once formed, rearranges back to **2**. On the other hand, the calculated barrier $\Delta G_{298\text{K}}^\ddagger = 21.2$ kcal/mol for the forward rearrangement $6 \rightarrow 7$ and the free energy difference between **6** and **7** $\Delta\Delta G_{298\text{K}} = 3.0$ kcal/mol agree well with the measured inner-phase barrier $\Delta G_{267\text{K}}^\ddagger = 20 \pm 0.5$ kcal/mol and equilibrium ratio $[\text{7}]/[\text{6}] = 5$, which equals $\Delta G_{298\text{K}} = 1$ kcal/mol.

Properties of Encapsulated Triplet Phenylnitrene ^3PN . In order to investigate the reactivity of encapsulated triplet phenylnitrene, we followed the photolysis of $\text{H}\odot\text{1}$ by UV/vis spectroscopy. Triplet phenylnitrene has a very characteristic absorption spectrum that extends far into the visible range with absorption bands at λ_{max} 303, 380, and 488 nm in EPA at 77

Chart 1

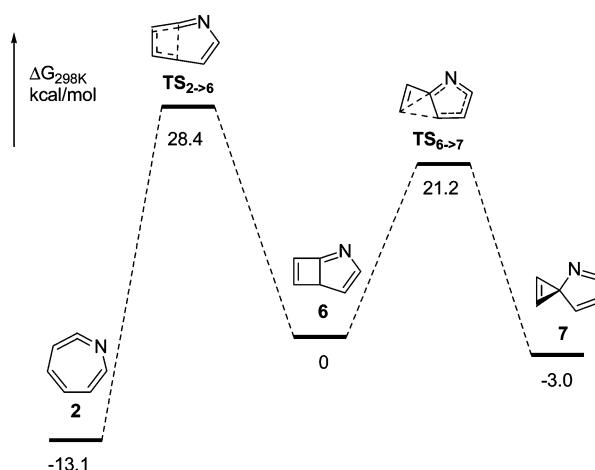
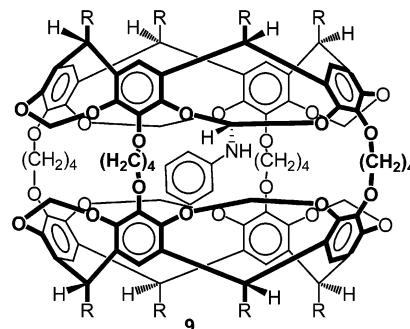
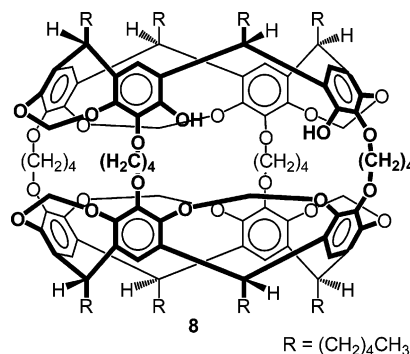


Figure 6. Calculated free energy diagram for the $2 \rightarrow 6 \rightarrow 7$ isomerization including transition states at the B3LYP/6-311G(d) level of theory.

K.³⁹ Photolysis of $\text{H}\odot\text{1}$ in degassed CH_2Cl_2 at -83 to -84 $^\circ\text{C}$ produced a deep-yellow solution. The color persisted for days at low temperature, but faded within several minutes upon warm-up to room temperature. Figure 7 shows a difference UV/vis spectrum of a briefly irradiated solution of $\text{H}\odot\text{1}$ in CH_2Cl_2 ($\lambda > 320$ nm; -74 $^\circ\text{C}$) recorded immediately after photolysis and 103 min later. At this temperature, photolysis of **1** produces primarily **2** and small amounts of ^3PN .^{11,19} The former has a lifetime of $\tau \approx 15$ min at this temperature and irreversibly rearranges to ^3PN .¹⁹ Thus, the spectrum shown in Figure 7 represents the difference in the absorption properties between encapsulated **2** and ^3PN .⁴⁰ The maxima of the positive bands at 305, 389, and 485 nm (indicated with arrows in Figure 7) are assigned to the major transitions of encapsulated triplet ^3PN .⁴⁰ When an irradiated solution was warmed up to -10.8 $^\circ\text{C}$,

(37) Since **6** and **7** rapidly equilibrate at room temperature, the acid-sensitivity of **6** could also be responsible for the decomposition of $\text{H}\odot\text{7}$.

(38) (a) Cram, D. J.; Tanner, M. E.; Knobler, C. B. *J. Am. Chem. Soc.* **1991**, *113*, 7717–7727. (b) Warmuth, R.; Maverick, E. F.; Knobler, C. B.; Cram, D. J. *J. Org. Chem.* **2003**, *68*, 2077–2088.

(39) EPA: Five parts diethyl ether, five parts isopentane, two parts ethanol.

(40) For a detailed discussion of the UV/Vis spectrum of ^3PN see ref 11b.

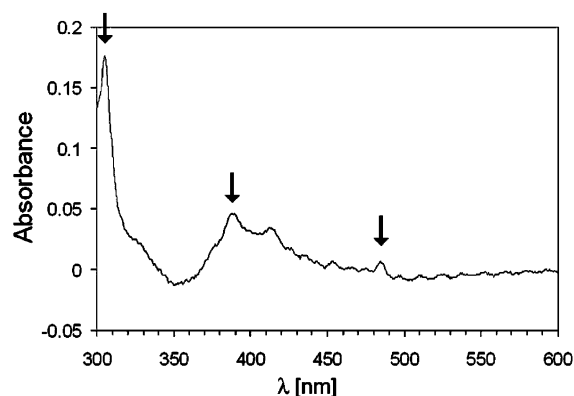


Figure 7. Difference UV/vis spectrum generated by subtracting the UV/vis spectrum of an irradiated solution of **H⊙1** (in CH_2Cl_2 ; -74°C) recorded 103 min after irradiation from that of the same solution recorded immediately after irradiation ($\lambda > 320$ nm). Arrows indicate λ_{max} of **H⊙³PN** at 306, 388, and 487 nm.

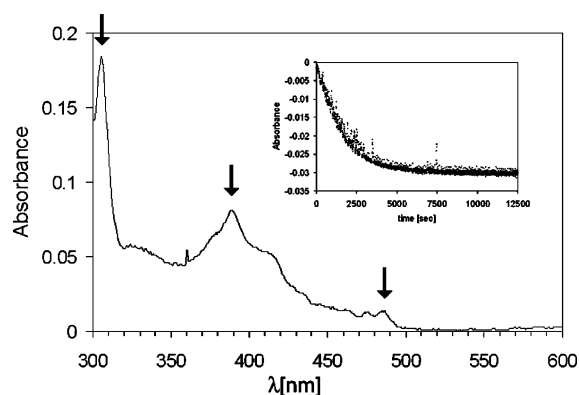


Figure 8. UV/vis absorption spectrum of encapsulated **³PN** at -10.8°C produced by irradiation of **H⊙1** in CH_2Cl_2 at -90°C ($\lambda > 320$ nm). Arrows indicate $\lambda_{\text{max}} = 306, 389,$ and 487 nm of **H⊙³PN**. (Insert) Exponential decay of the absorbance at $\lambda = 388$ nm.

H⊙³PN decayed with a rate constant of $4.3 \times 10^{-4} \text{ s}^{-1}$ as determined from the exponential decrease of the absorption at 387 nm (Figure 8 insert). A clearer UV/vis spectrum of encapsulated **³PN** is produced by subtraction of the spectrum recorded after decay of **H⊙³PN** from that of the solution immediately after warm-up (Figure 8). This spectrum is nearly superimposable with that of free **³PN** in EPA at 77 K,⁹ which supports our interpretation. The small red-shift of the absorption bands of encapsulated **³PN** relative to those of **³PN** in EPA are likely due to the different media and temperatures.⁴¹

From the temperature dependence of the rate of **H⊙³PN** decay between -3°C and -18°C , we determined the activation energy of $E_a = 13.3 \pm 0.5 \text{ kcal/mol}$ and pre-exponential factor of $A = 10^{7.7 \pm 0.4} \text{ s}^{-1}$ (Figure 9).⁴²

Even though the lifetime of encapsulated **³PN** is long at elevated temperatures ($\tau = 13.6$ min at -3°C), it can only be produced directly via photolysis of **H⊙1** at low temperature. The UV/vis spectrum of the photoproducts generated upon brief

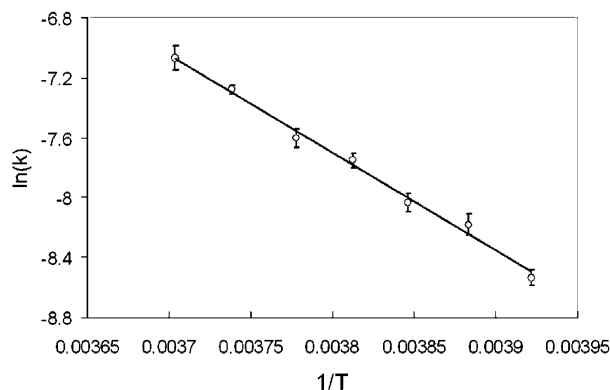


Figure 9. Arrhenius plot for the decay of encapsulated triplet phenylnitrene.

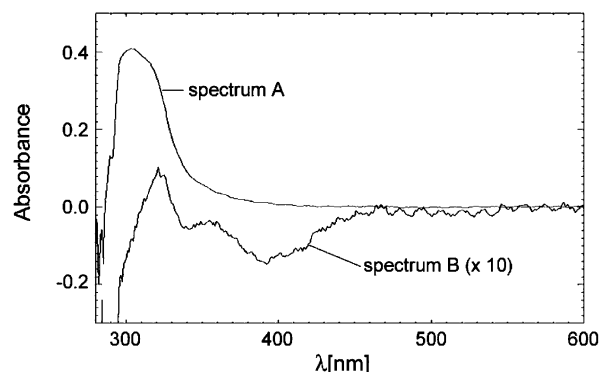


Figure 10. Difference UV/vis spectra of **H⊙1** in CH_2Cl_2 (-13°C). Spectrum A: before and immediately after brief irradiation ($\lambda > 320$ nm; -13°C); Spectrum B: immediately after irradiation and after warming to 17°C for 10 min.

irradiation ($\lambda > 320$ nm; 10 min) of **H⊙1** at -13°C is shown in Figure 10 (spectrum A). It lacks the characteristic absorption features of **³PN**. The minimal spectral changes observed after warming the photolyzed solution to 17°C for 10 min suggest that only trace amounts of **H⊙³PN**, if at all, were produced during the photolysis at -13°C (Figure 10, spectrum B). A logical interpretation is that **¹PN** reacts faster with the surrounding **H** than it intersystem crosses to **³PN**. The temperature-independent intersystem crossing rate constant of **³PN** is $k_{\text{ISC}} = 3.2 \pm 0.3 \times 10^6 \text{ s}^{-1}$ in pentane. It is presumably of the same magnitude inside **H** and sets the lower limit for the unimolecular rate constant of the reaction of **¹PN** with the surrounding **H**.^{11b} Thus, encapsulated **¹PN** must be at least 10 orders of magnitude more reactive than **³PN**. On the other hand, our low-temperature photolysis shows that the situation is different below -74°C , where temperature-independent intersystem crossing is faster than any reaction of **¹PN** with **H**.

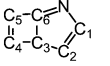
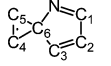
Discussion

Photochemical Rearrangement of Encapsulated Didehydroazepine 2. In previous work, we showed that photolysis of phenylazide **1** in the inner phase of hemicarceand **H** between -75 and -99°C produces didehydroazepine **2**, similar to the photochemistry **1** in solution in the same temperature range (Scheme 1). However, contrary to earlier photolysis experiments in solution, organic glasses, or inert gas matrices,^{3-7,9-14,15d,17-18} two new photoproducts formed in the inner-phase photolysis, which we identified as **H⊙6** and **H⊙7**. Hemicarceplex **H⊙6** is

(41) (a) Marquez, C.; Nau, W. M. *Angew. Chem., Int. Ed.* **2001**, *40*, 4387–4390. (b) Sánchez Carrera, S.; Brown, N.; Kerdellhué, J.-L.; Langenwalter, K. J.; Warmuth, R. *Eur. J. Org. Chem.* **2005**, 2239–2249.

(42) Standard errors were estimated by a linear least-squares regression of the Arrhenius plot; Bevington, P. R.; Robinson, D. K. *Data Reduction and Error Analysis for the Physical Sciences*; 2nd Ed., McGraw-Hill: New York, 1992; Chapter 6.

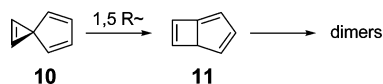
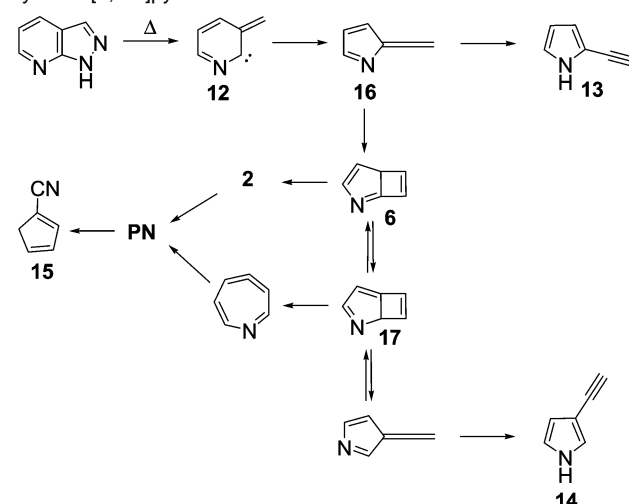
Table 3. Experimental and Calculated ^{13}C Chemical Shifts, δ_{exp} and δ_{calc} of Encapsulated **6** and **7**, Relative to Benzene in CDCl_3

										
$\delta_{\text{C,exp}}^{(b)}$	$\delta_{\text{C,calc}}^{(c)}$	$\delta_{\text{C,corr}}^{(c)}$	$\Delta\delta_{\text{C}}^{(d)}$	% $\Delta\delta_{\text{C}}^{(e)}$	$\delta_{\text{C,exp}}^{(f)}$	$\delta_{\text{C,calc}}^{(c)}$	$\delta_{\text{C,corr}}^{(c)}$	$\Delta\delta_{\text{C}}^{(d)}$	% $\Delta\delta_{\text{C}}^{(e)}$	
C1	154.4	160.9	156.9	4.0	2.5	161.5	165.2	164.0	1.2	0.7
C2	119.6	121.6	122.1	-0.5	-0.5	127.8	129.4	130.3	-0.9	-0.7
C3	73.0	74.5	75.5	-1.0	-1.5	153.1	159.5	155.6	3.9	2.5
C4	112.2	114.0	114.7	-0.8	-0.7	116.7	123.1	119.6	3.9	3.2
C5	137.5	144.8	140.0	4.8	3.4	116.7	123.1	119.6	3.9	3.2
C6	169.2	176.6	171.7	4.9	2.8	61.7	63.9	64.2	-0.3	-0.5

^a DFT-GIAO-chemical shift tensors (PBE1PBE/6-311G++(2d, p)//B3LYP/6-311G(d)) relative to benzene ($\delta_{\text{C}} = 128.37$ in CDCl_3).⁴⁴ ^b At 243 K. ^c $\delta_{\text{C,corr}} = \delta_{\text{C,exp}} + \text{host induced upfield shift} (\sim 2.5 \text{ ppm})$. ^d $\Delta\delta_{\text{C}} = \delta_{\text{C,comp}} - \delta_{\text{C,corr}}$. ^e % $\Delta\delta_{\text{C}} = \Delta\delta_{\text{C}}/\delta_{\text{C,corr}} \times 100$. ^f At 298 K.

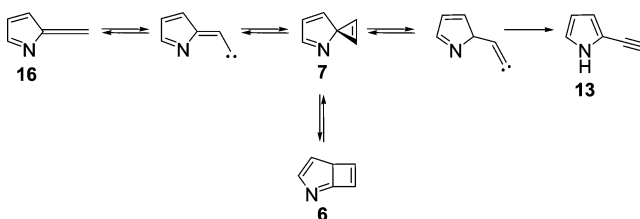
a secondary photoproduct of **H**⊙**2** and forms via an allowed photochemical four-electron electrocyclicization (Scheme 2). Hemarcerplex **H**⊙**7** is a secondary photoproduct of **H**⊙**6**. In addition, **6** and **7** interchange thermally through 1,5-sigmatropic shifts. The identity of both hemarcerplexes is supported by ^1H and ^{13}C 1D and 2D NMR experiments and IR spectroscopy. It mainly rests on the very good match between experimental and computed ^{13}C chemical shifts using the GIAO DFT method (Table 1) and the magnitude of direct ^{13}C – ^{13}C and ^{13}C – ^1H coupling constants (Figure 2). For both compounds, the GIAO DFT method overestimates the ^{13}C chemical shifts by about 5.9 to 11.8 ppm. A systematic overestimation of ^{13}C chemical shifts by this method has also been noted earlier by others.⁴³ However, strong improvement of the computed chemical shifts could be obtained by referencing to benzene instead of TMS. Likewise, when we used benzene as standard and an experimental chemical shift of $\delta_{\text{C}}(\text{benzene}) = 128.37$ (in CDCl_3), the computed ($\delta_{\text{C,calc}}$) ^{13}C chemical shifts ($\delta_{\text{C,exp}}$) of **6** and **7** matched the experimental shifts much more closely (Table 3).⁴⁴ If we further correct $\delta_{\text{C,exp}}$ for the 2–3 ppm hemarcerand-induced upfield shift,^{19,21c} the computed $\delta_{\text{C,calc}}$ and corrected experimental shifts $\delta_{\text{C,corr}}$ differ by less than 5 ppm (average 2.5 ppm) or 0.5 to 3.4% (Table 3).

Guest **6** is a highly strained anti-Bredt imine.⁴⁵ It is destabilized by cyclobutene ring strain and olefinic strain of the bridgehead imine bond, whereas **7** is destabilized by the spiro carbon and the cyclopropene ring strain.⁴⁵ The nearly equal energy of both shows that the sum of the destabilizing contributions of each compound are approximately the same. However, both are less stable than other spectroscopically observed species of the phenylnitrene rearrangement.^{15b, d} The 1,5-sigmatropic rearrangement of **6** to **7** is reminiscent of the chemistry of spirene **10**, which undergoes the reverse rearrangement to bicyclo[3.2.0]hepta-1,3,6-triene **11**.⁴⁶ The latter subsequently dimerizes.^{46a} The measured barrier for the rearrangement of **10** ($E_{\text{a}} = 24.7 \text{ kcal/mol}$) and the computed relative energy between **10** and **11** (0.5 kcal/mol) are very similar to the barrier for the rearrangement **7** → **6** ($21.0 \pm 0.5 \text{ kcal/mol}$) and the free energy difference between both.⁴⁷

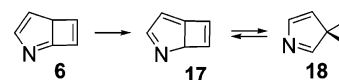
**Scheme 3.** Proposed Mechanism for the Pyrolysis of Pyrazolo[3,4-*b*]pyridine⁴⁷

Anti-Bredt imine **6** has earlier been postulated as intermediate in gas-phase pyrolysis experiments in order to explain the rearrangement of azamethylenecyclohexadienyldiene (**12**) to 2- (**13**), 3-ethynylpyrrole (**14**), and cyanocyclopentadiene (**15**) (Scheme 3).^{47–48}

In this thermal rearrangement, azaspirene **7** serves as a mechanistic link that connects azafulvenallene **16** with **13** and with **6** through known allene–vinylcarbene–cyclopropene and cyclopropene–vinylidene–methylacetylene rearrangements and the here described interconversion between **6** and **7**.⁴⁹



The possibility that **6** might in part undergo a 1,5 hydrogen shift leading to azabicyclo[3.2.0]heptatriene **17** and azaspirene **18** as minor products during the warm-up of a solution containing encapsulated **6** was dismissed on the basis of the computed activation free energy of 38.4 kcal/mol for this H-shift (B3LYP/6-311G(d)), which is substantially higher than the alternative rearrangement to **7** (Figure S7).



Interestingly, the rearrangements of **2** → **6** and **6** → **7** have not been observed in earlier photolysis of phenylazide. In

- (43) Buntkowsky, G.; Hoffmann, W.; Kupka, T.; Pasterna, G.; Jaworska, M.; Vieth, H.-M. *J. Phys. Chem. A* **1998**, *102*, 5794–5801.
 (44) Gottlieb, H. E.; Kotlyar, V.; Nudelman, A. *J. Org. Chem.* **1997**, *62*, 7512–7515.
 (45) Maier, W. F.; Schleyer, P. v. R. *J. Am. Chem. Soc.* **1981**, *103*, 1891–1900.
 (46) (a) Billups, W. E.; Saint, R. K.; Litosh, V. A.; Alemany, L. B.; Wilson, W. K.; Wiberg, K. B. *J. Org. Chem.* **2002**, *67*, 4436–4440. (b) Wong, M. W.; Wentrup, C. *J. Org. Chem.* **1996**, *61*, 7022–7029.
 (47) Wentrup, C. In *Reactive Intermediates*; Abramovitch, R. A., Ed.; Plenum Press: New York, 1980; Vol. 1, pp 263–319.
 (48) Crow, W. D.; Lea, A. R.; Paddon-Row, M. N. *Tetrahedron Lett.* **1972**, 2235–2238.
 (49) Walsh, R. *Chem. Soc. Rev.* **2005**, *34*, 714–732.

solution-phase photolysis around ambient temperature, this might be due to the transient nature of **2**. The lifetime of free **2** at room temperature in the absence of nucleophiles and at high dilution is approximately 5 ms and substantially shorter in the presence of nucleophiles or at higher concentration.^{10c,12} Thus, the photochemical electrocyclization of free **2** to **6** will require high light intensity to be observable at ambient temperature. However, it is surprising, that the rearrangement **2** → **6** → **7** has not been observed in matrix isolation studies, under which conditions **2** is thermally stable infinitely. Hayes and Sheridan photolyzed matrix-isolated **2** at 334 nm and produced ³PN.⁵ On the other hand, Chapman and LeRoux demonstrated that irradiation above 200 nm interconverts ³PN and 2-pyridylmethylene via **2** and observed that **2** is unstable toward irradiation above 360 nm, producing several photoproducts.⁴ Several possible reasons might account for the different products in matrices and the inner phase of **H**: (1) the different irradiation conditions (irradiation time, intensity, and wavelength); (2) the large temperature differences in both experiments. The excited-state rearrangement **2** → **6** might have a barrier that is too high to be surpassed at 10 K. However, inside the hemicarcerand at 190 K, **2** might slowly “leak” out of the **2** ⇌ ³PN photochemical equilibrium⁵ into the **6**, **7** manifold. (3) The hemicarcerand might further reinforce the latter effect, if there is indeed a barrier. The high polarizability of the inner phase of a hemicarcerand is known to lower activation energies by up to 2–3 kcal/mol via selective transition state stabilization.^{41,50} A stronger stabilization of the transition state leading to **6** as compared to that leading to **2** may make the excited-state rearrangement **2** → **6** observable in the inner phase of **H**.

Encapsulated Triplet Phenylnitrene. Inner-phase photolysis of **1** between –74 °C and –85 °C produces a mixture of encapsulated **2**, **6**, **7**, and ³PN. The formation of the former guests **2**, **6**, and **7** is supported by NMR spectroscopy of the reaction mixture. The formation of the latter guest is supported by the excellent match between its UV/vis spectrum and that reported for ³PN in EPA at 77 K. Furthermore, we show that the species assigned to ³PN is produced at –74 °C via the thermal decay of **2** as predicted by high level ab initio calculations^{15b–d} and in agreement with earlier experimental findings.¹⁰ Consistent with the formation of ³PN and its high stability inside **H** are also our low-temperature ¹³C NMR experiments. For example, no new guest ¹³C signals are generated as encapsulated ¹³C₆-**2** decays at –86 °C, which supports the formation of a stable paramagnetic species that does not react with the surrounding hemicarcerand at this temperature.⁵¹

Encapsulated ³PN slowly decays between 255 and 270 K with a rate constant $k = 10^{7.7 \pm 0.4} \text{ s}^{-1} \times \exp\{-13.3 \pm 0.5 \text{ kcal/mol}/RT\}$. We explain the high stability of encapsulated ³PN with the prevention of dimerization by the surrounding host. In solution, dimerization of ³PN is diffusion controlled.⁵¹ Long-lived arylnitrenes have earlier been generated photochemically in polymeric matrices, which also prevent dimerization of the

nitrene. Under these conditions, phenylnitrene decays through other pathways including C–H bond insertion. Reiser and Leyshon measured the room-temperature lifetime of ³PN ($\tau = 100 \text{ ms}$) inside a polystyrene matrix.²³ The extrapolated lifetime of **H**⊙³PN is approximately 800 times longer, which may be explained with the higher reactivity of the benzylic C–H bonds in polystyrene as opposed to the C–H bonds of **H** that point into the inner cavity. The isolation of substantial amounts of diol host **8**, which is the expected hydrolysis product of *N*-anilino-orthoformamide host **9**, suggests that **PN** preferentially inserts into an inward-pointing acetal C–H bond of the surrounding host. On the basis of our study, it is however not clear whether the lifetime of encapsulated ³PN is controlled entirely by the rate of its reaction with the surrounding host (e.g., C–H insertion) or alternatively by the rate of thermally activated intersystem crossing to the at least 10 orders of magnitude more reactive singlet ¹PN. In fact, the gas-phase phenylnitrene singlet–triplet energy gap $E_{\text{ST}} = 15 \text{ kcal/mol}$ is very close to the measured activation energy of the decay of encapsulated ³PN ($E_{\text{a}} = 13.3 \text{ kcal/mol}$).⁵³ Selective stabilization of ¹PN, whose unpaired electrons are more dispersed than in ³PN,¹⁵ by the surrounding host might lower E_{ST} slightly in the inner phase. Support for or against the latter mechanism of ³PN decay, which would provide a new method to measure E_{ST} , will require additional investigations with other substituted phenylnitrenes.

Conclusions

In conclusion, broadband ($\lambda > 320 \text{ nm}$) irradiation of hemicarceplex **H**⊙**1** between –74 °C and –84 °C, produces encapsulated didehydroazepine **2**, triplet phenylnitrene ³PN, 2-azabicyclo[3.2.0]hepta-1,3,6-triene **6**, and 4-azaspiro[2.4]hepta-1,4,6-triene **7**. The highly strained anti-Bredt imine **6** is formed from **2** via a photochemical four-electron electrocyclicization. Under the irradiation conditions, **6** rearranges further to azaspiroene **7**. Both imines interconvert thermally via 1,5-sigmatropic shifts yielding a final equilibrium of **7**/[**6**] = 5 at room temperature. The observation of a photochemical rearrangement of **2** to **6** contrasts earlier results of narrow band irradiations ($\lambda = 334 \text{ nm}$) of matrix-isolated **2**, which yields ³PN.⁵ Possible explanations are the different irradiation conditions (narrow band versus broadband irradiation), the different temperatures (8–10 K versus 190 K), and/or reaction environment (N₂ matrix versus inner phase) in both experiments. Encapsulated ³PN is remarkably stable due to the prevention of its dimerization by the surrounding hemicarcerand. Between 255 and 270 K, it decays with a rate constant $k = 10^{7.7 \pm 0.4} \text{ s}^{-1} \times \exp\{-13300 \pm 500 \text{ cal/mol}/RT\}$. The isolation of substantial amounts of a hemicarcerand lacking one acetal spanner suggests that ³PN decays preferentially by inserting into an inward-pointing acetal C–H bond of **H**. Rate limiting for the decay of encapsulated ³PN might be intersystem crossing to singlet phenylnitrene. Support for or against this decay mechanism awaits further experimental investigations.

Acknowledgment. We warmly thank the National Science Foundation for support of this research (Grants CHE-0431749 and CHE-0518351).

Supporting Information Available: ¹H, ¹³C, TOCSY NMR spectra of compound **8**. TOCSY and DQCOSY of photolyzed

(50) Warmuth, R.; Kerdelhué, J.-L.; Sánchez Carrera, S.; Langenwalter, K. J.; Brown, N. *Angew. Chem., Int. Ed.* **2002**, *41*, 96–99.

(51) See Figure 1d in ref 19.

(52) (a) Liang, T.-Y.; Schuster, G. B. *J. Am. Chem. Soc.* **1987**, *109*, 7803–7810.

(53) The gas-phase singlet–triplet gap of phenylnitrene has recently been remeasured. The most accurate value is $E_{\text{ST}} = 15 \text{ kcal/mol}$. Professor Paul G. Wenthold. Personal communication.

solutions of **H**⊙**1**. Tables with rate constants for the decay of **H**⊙**3PN** and with computed spin–spin coupling constants for **6** and **7** at the B3LYP/6311G++(2d, p) level. Energies and Cartesian coordinates of **2**, **6**, **7**, **17**, **18**, **TS**_{2→6}, **TS**_{6→7}, **TS**_{6→17}, and **TS**_{17→18} at the B3LYP/6-311G* level. GIAO chemical shift tensors (PBE1PBE/6-311G++(2d, p) for **6**, **7**, **17**, **18**, and tetramethylsilane (TMS) and Tables with calculated ¹³C chemi-

cal shifts of **6**, **7**, **17**, and **18**. Calculated free energy diagram for the **2** → **6** → **7** and **6** → **17** → **18** isomerizations including transition states at the B3LYP/6-311G(d) level. Complete reference 24. This material is available free of charge via the Internet at <http://pubs.acs.org>.

JA066130A